Applied Catalysis B: Environmental 125 (2012) 383–389

Contents lists available at SciVerse ScienceDirect

Applied Catalysis B: Environmental

journal homepage: www.elsevier.com/locate/apcatb

Synthesis of highly photoactive TiO_2 and Pt/TiO_2 nanocatalysts for substrate-specific photocatalytic applications

C. Fernández-Rodríguez[a,*], J.M. Doña-Rodríguez[a], O. González-Díaz[a], I. Seck[a], D. Zerbani[a], D. Portillo[b], J. Perez-Peña[a]

[a] Grupo de Fotocatálisis y Espectroscopía Aplicada al Medioambiente-FEAM (Unidad Asociada al Instituto de Ciencia de Materiales de Sevilla, C.S.I.C.), CIDIA-Depto. de Química, Edificio del Parque Científico Tecnológico, Universidad de Las Palmas de Gran Canaria, Campus Universitario de Tafira, 35017 Las Palmas, Spain
[b] Departamento de Química, Universidad de Zulia, Venezuela

ARTICLE INFO

Article history:
Received 31 October 2011
Received in revised form 20 April 2012
Accepted 27 April 2012
Available online 4 May 2012

Keywords:
Sol–gel synthesis
Pt/TiO_2
TiO_2
Specific-substrate photoactivity

ABSTRACT

The relative activity of TiO_2 photocatalysts depends to a large extent on the type of test substrate. With this in mind, phenol, formic acid, 2,4-dichlorophenoxyacetic acid (2,4-D) and methyl orange (MO) were selected as test substrates due to their different degradation mechanisms. In this work, the aim behind the synthesis and subsequent surface modification of the nanocatalysts was to obtain the most efficient material for removing these test substrates from water. A series of nanocatalysts with different average particle size, specific surface area and anatase phase content were synthesized by sol–gel method followed by calcinations at different annealing temperatures or hydrothermal treatment. Subsequently, platinization of certain samples was carried out using a photodeposition method. The most efficient catalyst for phenol photodegradation was found to be that with the largest average particle size as well as the highest anatase phase ratio. The photodeposition of platinum on this sample had detrimental effects on phenol photodegradation. The platinized sample and anatase TiO_2 with the lowest average particle size were the most efficient catalysts for the removal of formic acid. Finally, the platinized material also showed the highest photoactivity in the removal of 2,4-D and in the methyl orange bleaching test.

1. Introduction

TiO_2 is the most preferable material for the heterogeneous photocatalytic processes due to its high photoactivity, non-toxic nature, large band-gap and stability [1,2]. Despite the positive attributes of TiO_2, there are some drawbacks associated with its use: (i) charge carrier recombination occurs within nanoseconds [3–5] and (ii) the band edge absorption threshold does not allow the utilization of visible light [6]. To avoid these particular limitations, a number of strategies have been proposed to improve the light absorption features and lengthen the carrier life time. Surface modification of TiO_2 with a number of organic dyes extends the sensitivity of TiO_2 in the visible region [7–11]. Non-metal [12–16] or metal [17–26] doping could produce band-gap narrowing or localized mid-gap states extending the photoactivity to the visible region. Coupling TiO_2 with narrow band gap semiconductors which are able to absorb visible light and inject electrons into the conduction band (CB) of titania also extends the photoactivity to the visible range [27–30]. Another strategy proposed to enhance the visible photoactivity is the synthesis of reduced TiO_2 with oxygen vacancy states between the TiO_2 valence and conduction bands or the synthesis of anatase particles with oxygen sub-stoichiometry [31–33]. Transition or rare-earth metal doping in the crystalline structure could significantly influence charge carrier recombination rates and interfacial electron-transfer rates [34,35]. Another approach to increase the efficiency of charge separation involves the contact of the semiconductor particles with another semiconductor [36–38]. Noble metals can also be loaded on the semiconductor surface to solve this problem. Many researchers have demonstrated that the photocatalytic activity may be enhanced by impregnating the surface of titanium dioxide with noble metals [39–41]. Finally, another strategy used is the synthesis of pure anatase with high crystallinity and large average particle size. In this case, the photocatalysts exhibit a low density of surface defects where the surface recombination rate of electrons and holes is diminished [42]. However, TiO_2 samples with larger average particle size and lower specific surface area could have a negative effect on photocatalytic activity by reducing the amount of adsorbed reactants. Previous study has demonstrated that the relative activity of photocatalysts with different specific surface area depends to a large extent on the kind of test substrate [43]. It is clear that the substrates that can be appreciably adsorbed on the TiO_2 surface can be oxidized directly by

* Corresponding author at: Parque científico-tecnológico (U.L.P.G.C.), Ed. Polivalente I. 1ª Planta, 35017 Campus de Tafira, Las Palmas de Gran Canaria, Las Palmas, Spain. Tel.: +34 928 452989; fax: +34 928 457397.
E-mail address: cfernandez@proyinves.ulpgc.es (C. Fernández-Rodríguez).

0926-3373/$ – see front matter © 2012 Published by Elsevier B.V.
http://dx.doi.org/10.1016/j.apcatb.2012.04.042

holes or by adsorbed •OH radicals, or can be reduced by photogenerated electrons. However, non-adsorbed substrates can only be oxidized or reduced through the participation of radicals such as •OH, $•O_2^{2-}$ and •H. It has been reported that the most efficient TiO_2 photocatalysts in the degradation of non-adsorbed substrates on the TiO_2 surface are those with large particle size, high crystallinity and high anatase phase content [44]. In addition, •OH radical formation on TiO_2 samples increases as the annealing temperature rises and is associated with the increase in crystallite size and the decrease in the lattice strain of anatase particles. This •OH radical formation decreases gradually after anatase to rutile phase transformation by over 9% in mass [45]. However, the efficiency of the catalysts improves as the specific surface area increases in the case of molecules appreciably adsorbed on the TiO_2 surface [46]. Therefore, when addressing the synthesis of an efficient photocatalyst its efficiency should not be assessed by the photocatalytic degradation of a single type of substrate. TiO_2 photoactivity needs to be tested on a variety of substrates which are degraded through different photocatalytic mechanisms.

With this in mind, phenol and formic acid were selected as substrates since these compounds are degraded by the two photocatalytic mechanisms described previously. In addition, dichlorophenoxyacetic acid (2,4-D) and methyl orange (MO) were also selected as substrates as 2,4-D can be degraded by both mechanisms, although it does so primarily by photogenerated holes [47], while MO presents an interesting photoreduction mechanism [48] on the surface of the photocatalyst.

So, synthesis was primarily aimed at obtaining materials with high and similar average particle size, low specific surface area and different anatase phase ratio. The efficiency of these photocatalysts was tested on phenol photodegradation. In addition, the amorphous material from the best catalyst to photodegrade phenol was annealed at lower temperatures or subjected to a hydrothermal treatment in order to obtain materials with higher specific surface area and smaller average particle size. The efficiency of all these photocatalysts was tested on the different substrates chosen to try to verify whether photocatalysts with higher specific surface area values were in fact more effective on the photodegradation of strongly adsorbed substrates.

Finally, platinized modification of samples with low surface defect density was performed by photodeposition in order to inhibit the undesired electron–hole recombination, thereby facilitating the direct oxidation by photogenerated holes of molecules appreciably adsorbed on the TiO_2 surface and improving the photo-generated electron transfer from the catalyst to adsorbed substrates.

These new catalysts were characterized by means of transmission electron microscopy (TEM), BET specific surface area measurements, diffuse reflectance spectroscopy (DRS) and X-ray diffraction (XRD).

2. Experimental

2.1. Preparation of the catalysts

The photocatalysts were synthesized following a sol–gel procedure. For this, a solution containing 40 mL ethanol (99.5% Panreac) and 17 mL titanium butoxide (97% Sigma–Aldrich) was added drop by drop to 15 mL of acidic ultrapure water at pH 1.82 and 40 mL of ethanol. Nitric acid (N) (60% Panreac), acetic acid (A) (99.5% Paneac) and citric acid (C) (99.5% Panreac) were tested as acids. The mixing time was 2 h. After this, the final solution was stirred for 30 min and then allowed to age for 48 h. Then, the catalysts were dried at 373 K for 24 h. Subsequent to this aging and drying treatment, sieving was carried out using a 63 μm mesh size. For hydrothermal treatment, amorphous TiO_2 and 100 mL of ultrapure water were placed in an autoclave at 423 K for 24 h. For annealing treatment, catalysts were placed on porcelain capsules. A temperature programme with slope of 302 K/h was used and the final temperature was held for 3.5 h. Three annealing temperatures of 773, 873 and 1023 K were tested. The platinized sample was prepared by metal photodeposition following a method previously reported [49]. Pt doping was achieved using hexachloroplatinic (IV) acid (H_2PtCl_6, Sigma–Aldrich 37.5% Pt). Solutions of H_2PtCl_6 (corresponding to a 1.0 wt% metal loading) in distilled water were prepared and mixed with suspensions of the TiO_2 in distilled water (1 g TiO_2 L^{-1}), adding isopropanol (98.5% Panreac) as sacrificial donor (0.3 M final concentration). Photodeposition was performed by illuminating the suspensions for 6 h with a medium pressure mercury lamp (400 W) of photon flux ca. 2.6×10^{-7} einstein s^{-1} L^{-1} in the <400 nm region while maintaining continuous nitrogen purging. The product was then recovered by centrifugation and dried at 110 °C overnight. The synthesized photocatalysts were denoted as E(A, N or C)T followed by calcination temperature or HT for hydrothermal sample and *t*. The commercial catalyst Degussa P25 was provided by *Degussa* AG (Germany).

2.2. Equipment and techniques

A JEOL electron microscope was employed for transmission electron microscopy (TEM) analyses. The microscope was equipped with a top-entry holder and ion pumping system operating at an accelerating voltage of 200 kV and providing a nominal structural resolution of 0.21 nm. Samples were prepared by dipping a 3 mm holed carbon grid into the catalyst suspended in ethanol. Finally, the grids were dried at 323 K for 5 min.

BET specific surface area measurements were carried out by N_2 adsorption at 77 K using a Micromeritics Gemini instrument.

UV–Vis spectra were measured on a Cary 5 (Varian) apparatus, equipped with an integrating sphere, and using Poly Tetra Fluoro Ethylene (PTFE) as reference. PTFE is considered an important material in reflectance studies for its physical and chemical properties. The spectra were recorded in diffuse reflectance mode and transformed to a magnitude proportional to the extinction coefficient (K) by means of the Kubelka–Munk function ($F(R_\infty)$). The band gap values were obtained under the assumption of indirect transition for all tested photocatalysts.

X-ray diffraction (XRD) patterns were obtained by using a Siemens D-500 diffractometer (Cu Kα, λ = 1.5432 Å). Crystallite sizes in the different phases were estimated from the line broadening of the corresponding X-ray diffraction peaks by using the Scherrer equation. Peaks were fitted by using a Voigt function.

A 60 W Solarium Philips HB175 equipped with four 15 W Philips CLEO fluorescent tubes with emission spectrum from 300 to 400 nm (maximum around 365 nm, 9 mW) was used as UV source. Remaining phenol and 2,4-D concentrations at different reaction times were HPLC-measured using a Supelco Discovery C18 25 cm × 4.6 mm ID, 5 μm particle column and an acetonitrile–water solution as mobile phase (20:80, v:v), using a Diode Array Detector (DAD) (λ = 270 nm) for analysis of phenol, and methanol–25 mM phosphate buffer pH 2.3 aqueous solution (70:30, v:v) as mobile phase and λ = 214 nm for 2,4-D analysis. The photocatalytic degradation rates of formic acid were determined by monitoring the reduction of total organic carbon (TOC) with a TOC analyzer (TOC-VCSH, Shimadzu). The color bleaching of MO was monitored by measuring the absorbance with a UV–Vis spectrophotometer (Thermo Helios-Gamma) at 465 nm.

Table 1
Crystalline phase, average particle sizes, percentage of anatase phase, specific surface area and band-gap for the different catalysts obtained by different synthesis ways.

Sample	Treatment	Crystallite size (nm)		% anatase	Surface area ($m^2\ g^{-1}$)	Band-gap (eV)
		Anatase	Rutile			
EAT-1023*t*	Acetic acid – calcined at 1023 K	58.1	133.8	14	17.3	2.87
ENT-1023*t*	Nitric acid – calcined at 1023 K	61.3	84.8	35	19.3	2.87
ECT-1023*t*	Citric acid – calcined at 1023 K	57.0	86.3	91.5	18.1	2.97
ECT-HT*t*	Citric acid - hydrothermal 423 K – 24 h	6.8	–	100	170.4	3.10
ECT-773*t*	Citric acid – calcined at 773 K	21.7	–	100	38.8	3.19
ECT-873*t*	Citric acid – calcined at 873 K	36.9	–	100	27.9	3.17
ECT-1023*t*-Pt	Citric acid – calcined at 1023 K – photodeposition of Pt	57.0	86.3	90	15.8	2.67
P25	–	21	33	80	50	3.18

2.3. Reaction conditions

Aqueous suspensions containing 0.53 mM of phenol or 2,4-D, 1 mM of formic acid or 0.053 mM of MO were selected as initial concentrations and 1 g/L catalysts in 250 mL glass vessels were continuously stirred and air-bubbled (400 mL/min). Experiments were performed at optimal pH for degradation and mineralization of tested substrates. Experiments at constant pH of 3, 5, 7 and 9 were carried out in order to determine the optimal pH for the given substrates. The optimal pH values for acidic compounds (formic acid, 2,4-D and MO) and phenol were 3 and 5, respectively. Organic chemisorption on the catalyst surface was favored by air-bubbling and stirring for 30 min before switching on the UV-lamp. The percentage of phenol photodegradation was determined after 60 min of reaction. Additionally, the percentage of phenol mineralization was determined after 120 min of reaction.

3. Results and discussion

3.1. Characterization studies

The structural and morphological properties of the samples prepared using different acids are presented in Table 1.

The ability to obtain TiO_2 samples with similar particle size of anatase phase and different ratio of anatase/rutile was attained using three different acids (acetic, nitric and citric) in the method of synthesis. TiO_2 containing high percentages of anatase phase (91%) was obtained by adding citric acid. On the contrary, particles with only 35% and 14% of anatase phase were obtained when nitric acid or acetic acid was added to the solution, respectively. Complexation of alkoxide precursors by chelating agents such as carboxylic acid permits control of the reactivity by avoiding fast hydrolysis/condensation of the precursors in contact with water [50]. In this method of synthesis, slow hydrolysis/condensation occurs when acetic acid is added favoring the presence of low-weight oligomeric species in solution. The transformation of rutile crystallites of this sample might be favored by the nanostructure of the initial titania particles. However, a rapid precipitation of TiO_2 is observed in the synthesis with citric acid. Hence, large aggregates of nanoparticles are rapidly yielded. A previous study showed that pure anatase titania could be obtained after the addition of citric acid to $TiCl_4$ aqueous solution under hydrothermal conditions. Meanwhile pure rutile crystallites were obtained with the addition of acetic acid [51]. It is noteworthy that large particle size of anatase phase is crucial to photodegraded efficiently substrates via hydroxyl radicals. Colón et al. [52] were able to obtain materials with 93% of anatase phase at 973 K by using sulfuric acid. However, in contrast with the average particle size obtained in this work (57 nm), they obtained an average anatase particle size of only 33.57 nm. It can therefore be concluded that the use of different acid leads to the synthesis of TiO_2 materials with high particle size and different anatase phase content at high calcination temperatures.

Subsequently, photocatalysts with lower average particle size (larger specific surface area) were obtained by subjecting the amorphous sample from the sol–gel process (ECT, amorphous TiO_2) to hydrothermal treatment or to lower calcination temperatures.

The results of the structural characterization of these synthesized catalysts are also presented in Table 1, as well as that of commercial Degussa P25 as reference. Fig. 1 shows the XRD patterns of samples ECT and P25.

It can be observed in Fig. 1 that crystallinity for the anatase phase increases as the calcination temperature of the ECT samples rises. The samples that underwent hydrothermal treatment showed the lowest crystallinity at this phase.

In a previous study, the commercial catalyst ST-01 (TiO_2 anatase phase, average particle size of 7 nm, Ishihara-Sangyo, Japan) was calcined at different temperatures, and showed that as the degree of crystallinity increased so did the methylene blue (MB) photodegradation rate [55]. In another study with photocatalysts of high crystallinity and average particle size smaller than that of P25, it was also reported that as the degree of crystallinity increased the MB and phenol photodegradation rates also rose [56]. A comparative study of various materials with the same average particle size but with different morphology showed that the more faceted the particles of TiO_2 (less spherical) the higher the photoactivity on the phenol degradation [57]. According to this, the high degree of crystallinity and faceted polyhedral structure observed in calcined materials (Fig. 2) could be positive attributes for their conversion into highly photoactive materials.

In the TEM image of ECT-1023-Pt sample it was observed that platinum clusters were homogeneously distributed on the photocatalyst surface. The average particle size and the percentage of dispension for the platinum nanoparticles were 4.03 nm and 42.5%, respectively. In two previous studies, deposition of platinum on P25 surface was carried out by using photodeposition method. The estimated range of Pt particle sizes (nm) obtained was 4–6 nm and 2–5 nm, respectively [53,54]

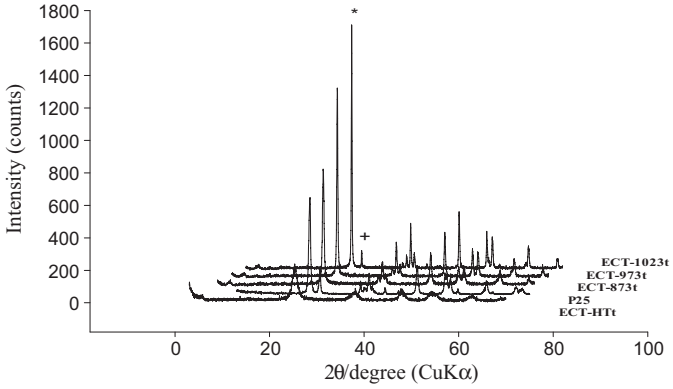

Fig. 1. XRD patterns of different ECT and P25 samples. The peaks marked * and + represent the anatase face [1 0 1] and rutile face [1 1 0] respectively.

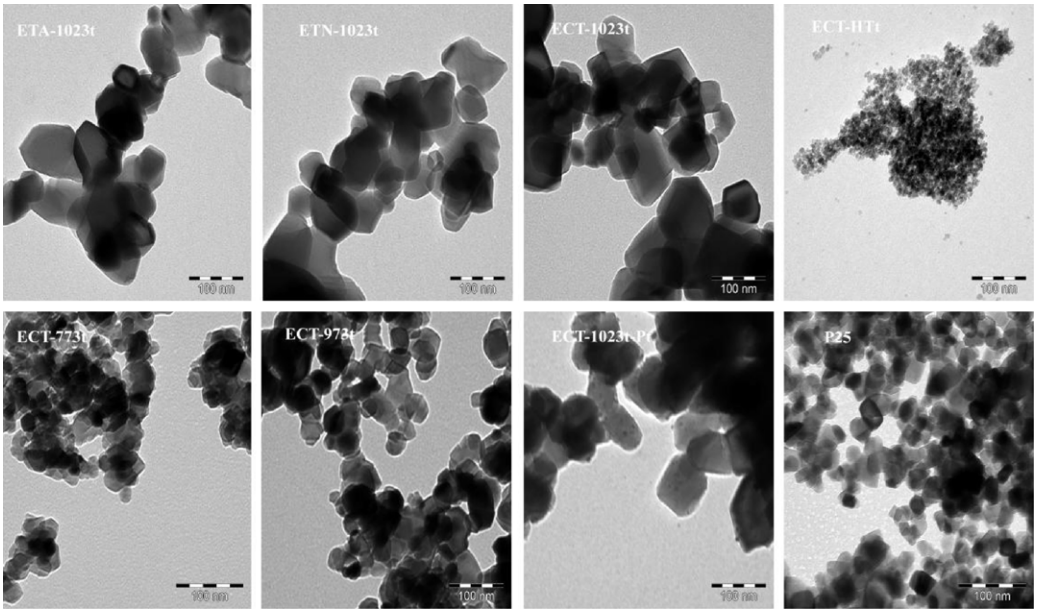

Fig. 2. TEM images of home-made TiO_2 and Degussa P25.

3.2. Photocatalytic experiments

3.2.1. Photoactivity on phenol decomposition

Table 2 shows the percentage of phenol degradation and mineralization at $t = 60$ and 120 min, respectively, using the different catalysts synthesized in this work in the presence of different acids. The results indicate that the most photoactive material for phenol degradation and mineralization was the catalyst where citric acid was used to adjust pH in the method of synthesis. It should be noted that ENT-1023*t* presented a relatively high activity despite its low anatase phase content (35%). The mineralization rate for phenol followed a similar activity pattern to that of the degradation rate. These results correlate with those obtained in a previous study where different anatase–rutile ratios in TiO_2 photocatalysts were prepared by using different HCl–$TiCl_4$ mixtures. In the aforementioned study, the photocatalytic performance of the samples in the phenol decomposition correlates well with their anatase content: photocatalysts containing only anatase as crystalline phase were up to three times more efficient than rutile-only ones [58].

In Fig. 3, the relative concentration of phenol and total organic carbon in the solution is plotted against irradiation time of UV rays for ECT samples. The performance in the presence of P25 is also shown in the figure as a reference. The higher photoactivity of ECT-1023*t* catalyst in the phenol degradation with respect to the other two catalysts calcined at 773 K and 873 K has been reported by our group in a previous study [59]. The results obtained using ECT-HT*t* which specific surface area is much higher than the annealed materials confirmed that phenol is degraded more efficiently by materials with a larger particle size and higher crystallinity.

Table 2
The percentage of phenol degradation at 60 min of irradiation time and the percentage of phenol mineralization at 120 min with the synthesized catalysts by using different acids and calcined at 1023 K.

Sample	% phenol photodegradation ($t = 60$ min)	% phenol mineralization ($t = 120$ min)
EAT-1023*t*	59.0	18.4
ENT-1023*t*	83.7	72.1
ECT-1023*t*	95.2	86.8
P25	84.4	84.1

In relation to the platinized sample, the platinum deposition on the catalyst with the highest particle size and a small percentage of rutile phase (8.5%), ECT-1023*t*, produced an inhibitory effect on phenol degradation. However, platinum deposition on pure anatase ECT-673*t* catalyst increased the degradation rate (r_o) of phenol from 0.5 to 1.67 (10^{-04} mol s^{-1}). Previous articles have also reported an inhibitory effect on phenol photocatalytic

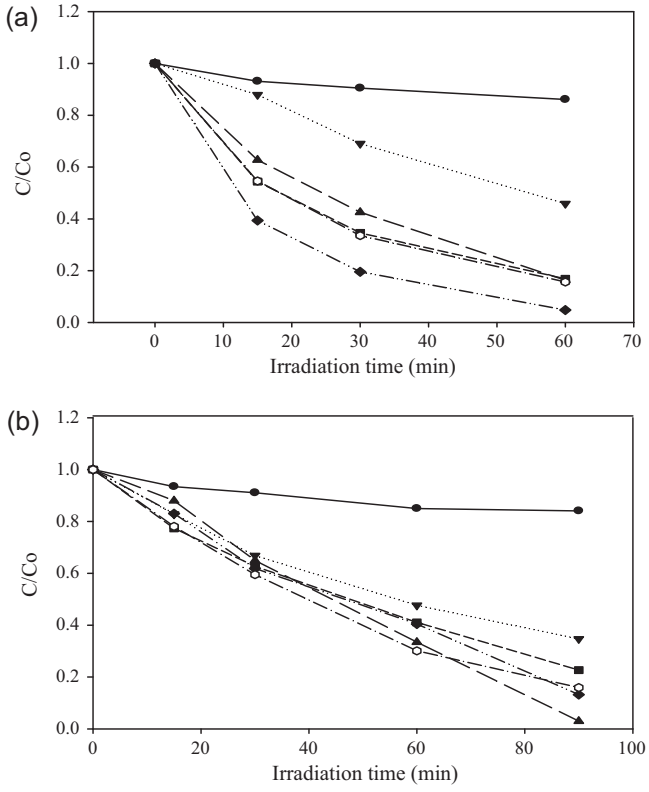

Fig. 3. Relative concentration profile for the photocatalytic decomposition (a) and the mineralization one for phenol (b), in the presence of different TiO_2 photocatalysts. (●) ECT-HT*t*; (▼) ECT-773*t*; (■) ECT-873*t*;(○) P25; (▲) ECT1023*t*-Pt and (♦) ECT-1023*t*.

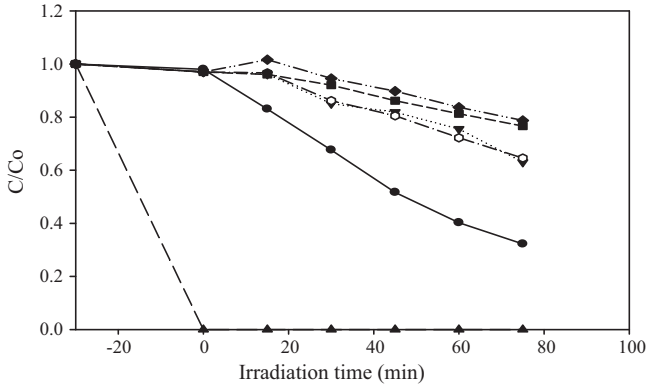

Fig. 4. Relative concentration profile for the photocatalytic decomposition of formic acid on different TiO_2 photocatalysts: (●) ECT-HT*t*; (▼) ECT-773*t*; (■) ECT-873*t*; (○) P25; (▲) ECT-1023*t*-Pt and (♦) ECT-1023*t*.

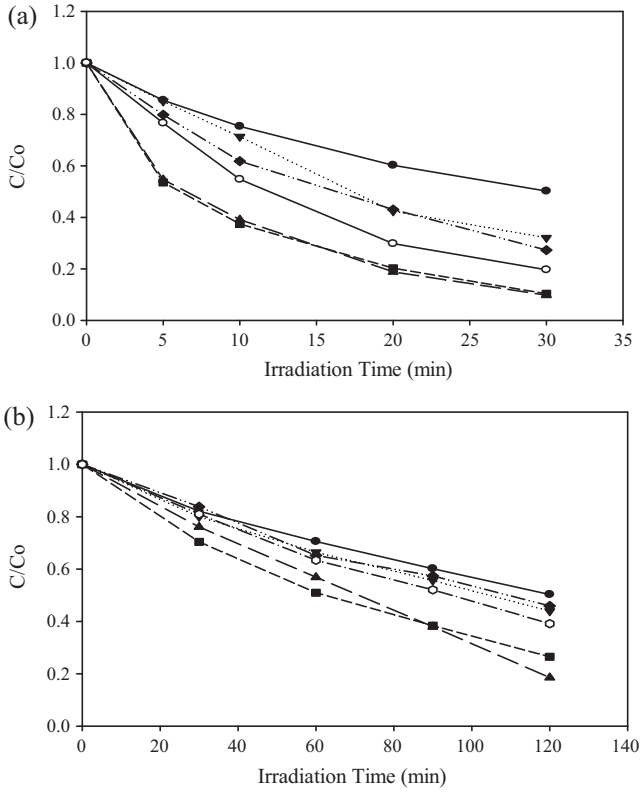

Fig. 5. Relative concentration profile for the photocatalytic decomposition (a) and the mineralization (b) for 2,4-D, using different TiO_2 photocatalysts. (●) ECT-HT*t*; (▼) ECT-773*t*; (■) ECT-873*t*; (○) P25; (▲) ECT-1023*t*-Pt and (♦) ECT-1023*t*.

oxidation due to the deposition of platinum on Degussa P25 [60]. In this work, this fact was attributed to platinum being unable to further increase the efficiency of charge separation by the capture of electrons and reduction of oxygen, since the junction between the two anatase and rutile phases already provides an optimum path for electron–hole separation. Holes are concentrated in rutile and electrons are left in anatase particles [61,62] before migration to the corresponding particle surface, and probably for this reason platinization did not produce any improvement of the photocatalyst activity for phenol photooxidation. However, the order of catalysts photoactivity in phenol mineralization after 90 min of reaction (Fig. 3b) follows the sequence: ECT-HT*t* < ECT-773*t* < ECT-873*t* < P25 ≈ ECT-1023*t* < ECT-1023*t*-Pt. It is noteworthy that the mineralization rate increases for the platinized catalyst when the remaining amount of phenol is very low. This may be due to the presence of platinum on ECT-1023*t* improves the photodegradation rate of certain intermediates such as short-chained aliphatic organic acids. Thus, the effect of platinum deposition on a specific catalyst must be evaluated by using different substrates such as it was carried out in this work.

3.2.2. Photoactivity on formic acid decomposition

In Fig. 4, the relative concentration of formic acid in the solution is plotted against irradiation time of UV rays for ECT samples. Photoactivity using P25 as a reference is also included. Total degradation of the tested concentration of formic acid with the catalyst ECT-1023*t*-Pt occurs even in the absence of light. Comparative experiment in inert atmosphere was carried out in order to check if oxidation is involved in this process or, as alternative, if the complete disappearance of formic acid from the liquid phase is just a consequence of pure adsorption. The results show that after 30 min, the formic acid concentration decreases to zero in the presence of air. On the contrary, the concentration of formic acid remains stable in nitrogen atmosphere. Catalytic wet air oxidation of other carboxylic acids in solutions over noble metal catalysts prepared on TiO_2 at 333 K and atmospheric pressure has already been reported in a previous study [63]. In relation to bare ECT catalysts, it can be observed that the photoactivity rises as the specific surface area increases. Therefore, the efficiency in formic acid photodegradation of catalyst obtained after hydrothermal treatment was considerably higher than those showed by calcined samples. These results agree with those obtained in a previous study where high specific surface area anatase samples were particularly active in formic acid degradation [64].

3.2.3. Photoactivity on 2,4-D decomposition

In Fig. 5a, the relative concentration of dichlorophenoxyacetic acid (2,4-D) in the solution is plotted against irradiation time of UV rays for ECT samples. It should be mentioned that the doped catalyst, contrary to what happened in the case of phenol degradation, showed higher efficiency than ECT-1023*t* in the photodegradation of this compound. In order to test the effect of platinization on a photocatalyst with a higher specific surface area, the same experiment was performed with Degussa P25. The same improvement was observed in the degradation rate of this compound. The photoplatinization of photocatalysts containing both main crystalline phases (anatase–rutile) could improve the photodegradation of molecules strongly adsorbed on the photocatalyst surface. This could explain why phenol mineralization rises significantly for irradiation times in which the intermediate organic acid concentration has fallen sharply, compared with short reaction times, as can be observed in Fig. 3b.

The most efficient of the non-platinized photocatalysts is the catalyst annealed at 873 K. The 2,4-D substrate can be degraded by both mechanisms through photogenerated h^+ or mobile $^{\bullet}OH$ radicals. Therefore, ECT-873*t* TiO_2, which has a moderately high average particle size (36.9 nm) and an intermediate specific surface area value (29.8 $m^2\,g^{-1}$), seems to have the best structural properties for efficient degradation of this substrate.

The comparison of the 2,4-D mineralization rate on the photocatalysts tested follows the same tendency as the degradation rate (Fig. 5b). However, the platinized sample showed a highest efficiency at longest time (120 min) since the concentration of the main intermediate of 2,4-D, 2,4-dichlorophenol has become zero at this time. This intermediate is a phenol derivative which is degraded poorly by this catalyst as it occurs in the case of phenol.

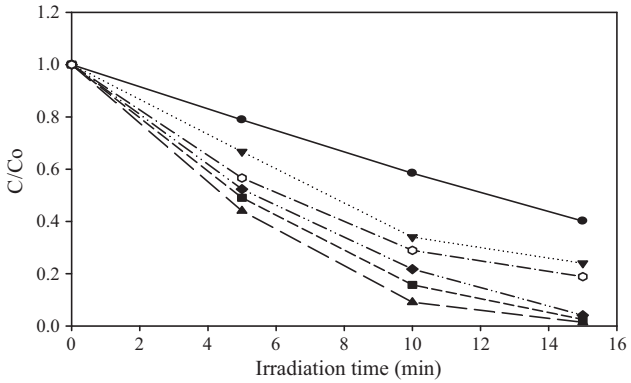

Fig. 6. Relative concentration profile for the photocatalytic decomposition of MO under anoxic conditions using different TiO_2 photocatalysts: (●) ECT-HT*t*; (▼) ECT-773*t*; (■) ECT-873*t*; (○) P25; (▲) ECT-1023*t*-Pt; (♦) ECT-1023*t*.

3.2.4. Photoactivity on MO decomposition

Fig. 6 shows the relative concentration of methyl orange (MO) in the solution against irradiation time of UV rays in the absence of air using ECT catalysts. Photoactivity in MO degradation follows the sequence: ECT-HT*t* < ECT-773*t* < P25 < ECT-1023*t* < ECT-873*t* < ECT-1023*t*-Pt.

Unsurprisingly, MO reduction is more effective when using platinized material due to the higher availability of photoelectrons to reduce the dye through the metal clusters (Eq. (1)). The photogenerated electrons reduce MO which results in the rupture of the azo-bond (Eq. (2)) and consequently the removal of dye color. In the case of the other photocatalysts, the photoactivity sequence is similar to that for 2,4-D. Thus, TiO_2 photocatalysts with moderate specific surface area and particle size are highly efficient at photodegrading substrates through photogenerated e^- such as methyl orange. In this case, no mineralization ensues because the MO photoreduction occurs without oxygen. Therefore, there are no intermediates produced by mineralization after azo-bond breakdown.

$$e^-_{cb} + Pt_{(dep)} \rightarrow Pt^-_{(dep)} \quad (1)$$

$$2Pt^-_{(dep)} + MO + 2H^+ \rightarrow 2Pt_{(dep)} + MOH_2 \quad (2)$$

4. Conclusions

This study clearly demonstrates that stabilization of TiO_2 anatase phase at a high calcination temperature (1023 K) is obtained by using citric acid in the sol–gel synthesis, whereas rutile transformation occurs when acetic acid or nitric acid is added and calcined at the same temperature. The TiO_2 photocatalyst with the highest crystallinity, particle size and anatase–rutile ratio (ECT-1023*t*) was the most photoactive material for the photodegradation of substrates such as phenol whose main photodegradation mechanism is via mobile •OH radicals. However, material prepared by hydrothermal treatment with lower particle size and higher area surface was more efficient at photodegrading substrates such as formic acid through photogenerated holes (h^+). Platinum clusters photodeposited on TiO_2 containing small percentage of rutile phase improved the photoactivity of bare TiO_2 for substrates whose degradation mechanism was via photogenerated e^- or h^+. In the case of phenol-type mechanisms, the photoactivity of this platinized material was lower when compared with bare TiO_2.

In conclusion, it is possible to design photocatalysts for specific substrates by tailoring the photocatalyst particle size, percentage of anatase phase, crystallinity and specific surface area by means of appropriate method of synthesis as well as thermal and mechanical post-synthesis treatments.

In future works the authors of this work will study the synergic and/or anti-synergic effects of the combination of different specific photocatalysts for the treatment of solutions containing substrate mixtures.

Acknowledgments

We are grateful for the funding of the European Commission through the Clean Water Project which is a Collaborative Project (Grant Agreement number 227017) co-funded by the Research DG of the European Commission within the joint RTD activities of the Environment and NMP Thematic Priorities. Furthermore, we would like to thank the Spanish Ministry of Science and Innovation for their financial support through the CTQ2008-05961-C02-02 and CTQ2008-05961-C02-01 Projects, the FONACIT of Venezuela for their financial support to Mr. D. Portillo and the Spanish Foreign Ministry for their financial support to Mr. I. Seck and Ms. D. Zerbani. Finally, special thanks go to Dr. J.A. Navio and Dr. A. Macias (University of Seville) for the DRX experiments and to Mr. J.M. Rodríguez from the TEM service of the University of Las Palmas de Gran Canaria.

References

[1] A. Fujishima, T.N. Rao, D.A. Tryk, Journal of Photochemistry and Photobiology C: Photochemistry Reviews 1 (2000) 1–21.
[2] U.I. Gaya, A.H. Abdullaha, Journal of Photochemistry and Photobiology C: Photochemistry Reviews 9 (2008) 1–12.
[3] M.R. Hoffmann, S. Martin, W. Choi, D.W. Bahnemann, Chemical Reviews 95 (1995) 69–96.
[4] A.I. Kokorin, D.W. Bahnemann, Chemical Physics of Nanostructured Semiconductors, VSP, Utrecht/Boston, 2003.
[5] R. Scotti, I.R. Bellobono, C. Canevali, C. Cannas, M. Catti, M. D'Arienzo, A. Musinu, S. Polizzi, M. Sommariva, A. Testino, F. Morazzoni, Chemistry of Materials 20 (2008) 4051–4061.
[6] J. Perkowski, S. Bzdon, A. Bulska, W.K. Józwiak, Polish Journal of Environmental Studies 15 (2003) 457–465.
[7] D. Chatterjee, S. Dasgupta, Journal of Photochemistry and Photobiology C: Photochemistry Review 6 (2–3) (2005) 186–205.
[8] D. Chatterjee, A. Mahata, Catalysis Communications 2 (2001) 1–3.
[9] D. Chatterjee, A. Mahata, Journal of Photochemistry and Photobiology A: Chemistry 153 (2002) 199–204.
[10] J. Moon, C.Y. Yun, K.W. Chung, M.S. Kang, J. Y, Catalysis Today 87 (2003) 77–86.
[11] S. Kaur, V. Singh, Ultrasonics Sonochemistry 14 (2007) 531–537.
[12] R. Asahi, T. Morikawa, T. Ohwaki, K. Aoki, Y. Taga, Science 293 (2001) 269–271.
[13] C. Burda, Y. Lou, X. Chen, A.C.S. Samia, J. Stout, J.L. Gole, NanoLetters 3 (2003) 1049–1051.
[14] J.L. Gole, J.D. Stout, C. Burda, Y. Lou, X. Chen, Journal of Physical Chemistry B 108 (2004) 1230–1240.
[15] C. Belver, R. Bellod, A. Fuerte, M. Fernández-García, Applied Catalysis B: Environmental 65 (2006) 301–308.
[16] C. Belver, R. Bellod, S.J. Stewart, F.G. Requejo, M. Fernández-García, Applied Catalysis B: Environmental 65 (2006) 309–314.
[17] M. Anpo, M. Takeuchi, Journal of Catalysis 216 (2003) 505–516.
[18] H. Yamashita, M. Harada, J. Misaka, M. Takeuchi, B. Neppolian, M. Anpo, Catalysis Today 84 (2003) 191–196.
[19] H. Yamashita, M. Harada, J. Misaka, M. Takeuchi, K. Ikeue, M. Anpo, Journal of Photochemistry and Photobiology A: Chemistry 148 (2002) 257–261.
[20] W.C. Hung, S.H. Fu, J.J. Tseng, H. Chu, T.H. Ko, Chemosphere 66 (2007) 2142–2151.
[21] M.S. Nahar, K. Hasegawa, S. Kagaya, Chemosphere 65 (2006) 1976–1982.
[22] P. Bouras, E. Stathatos, P. Lianos, Applied Catalysis B: Environmental 73 (2007) 51–59.
[23] Z. Ambrus, N. Balázs, T. Alapi, G. Wittmann, P. Sipos, A. Dombi, K. Mogyorósi, Applied Catalysis B: Environmental 81 (2008) 27–37.
[24] H. Li, G. Zhao, G. Han, B. Song, Surface and Coatings Technology 201 (2007) 7615–7618.
[25] D. Masih, H. Yoshitake, Y. Izumi, Applied Catalysis A-General 325 (2007) 276–282.
[26] X. Fan, X. Chen, S. Zhu, Z. Li, T. Yu, J. Ye, Z. Zou, Journal of Molecular Catalysis A: Chemical 284 (2008) 155–160.
[27] Y. Bessekhouad, D. Robert, J.V. Weber, Journal of Photochemistry and Photobiology A: Chemistry 163 (2004) 569–580.
[28] L. Wu, J.C. Yu, X. Fua, Journal of Molecular Catalysis A: Chemical 244 (2006) 25–32.
[29] W. Ho, J.C. Yu, Journal of Molecular Catalysis A: Chemical 247 (2006) 268–274.
[30] L. Jianhua, Y. Rong, L. Songmei, Rare Metals 25 (2006) 636–642.
[31] I. Nakamura, N. Negishi, S. Kutsuna, T. Ihara, S. Sugihara, K. Takeuch, Journal of Molecular Catalysis A: Chemical 161 (2000) 205–212.

[32] T. Ihara, M. Miyoshi, Y. Iriyama, O. Matsumoto, S. Sugihara, Applied Catalysis B: Environmental 42 (2003) 403–409.
[33] I. Justicia, G. Garcia, G.A. Battiston, R. Gerbasi, F. Ager, M. Guerra, J. Caixach, J.A. Pardo, J. Riverad, A. Figueras, Electrochimica Acta 50 (2005) 4605–4608.
[34] M.I. Litter, Applied Catalysis B: Environmental 23 (2–3) (1999) 89–114.
[35] A. Xu, Y. Gao, H. Liu, Journal of Catalysis 207 (2002) 151–157.
[36] K.Y. Song, M.K. Park, Y.T. Kwon, H.W. Lee, W.J. Chung, W.I. Lee, Chemistry of Materials 13 (7) (2001) 2349–2355.
[37] P.V. Kamat, Studies in Surface Science and Catalysis 103 (1997) 237–259.
[38] K. Vinodgopal, P.V. Kamat, Environmental Science and Technology 29 (1995) 841–845.
[39] D. Hufschmidt, D. Bahnemann, J.J. Testa, C.A. Emilio, M.I. Litter, Journal of Photochemistry and Photobiology A 148 (2002) 223–231.
[40] M.C. Hidalgo, M. Maicu, J.A. Navío, G. Colón, Catalysis Today 129 (2007) 43–49.
[41] M.C. Hidalgo, M. Maicu, J.A. Navío, G. Colón, Journal of Physical Chemistry C 113 (29) (2009) 12840–12847.
[42] M. Toyoda, Y. Nanbu, Y. Nakazawa, M. Hirano, M. Inagaki, Applied Catalysis B: Environmental 49 (2004) 227–232.
[43] J. Horyu, W.Y. Choi, Environmental Science and Technology 42 (2008) 294–300.
[44] A.G. Agrios, Pierre Pichat, Journal of Photochemistry and Photobiology A: Chemistry 180 (2006) 130–135.
[45] B. Tryba, M. Toyoda, A.W. Morawski, R. Nonaka, M. Inagaki, Applied Catalysis B: Environmental 71 (2007) 163–168.
[46] D.W. Bahnemann, S.N. Kholuiskaya, R. Dillert, A.I. Kulak, A.I. Kokorin, Applied Catalysis B: Environmental 36 (2002) 161–169.
[47] P. Kormali, A. Troupis, T. Triantis, A. Hiskia, E. Papaconstantinou, Catalysis Today 124 (2007) 149–155.
[48] T. Graham, Brown, R. James, Darwent, Journal of the Chemical Society-Faraday Transactions 1 (80) (1984) 1631–1643.
[49] M. Maicu, M.C. Hidalgo, G. Colón, J.A. Navío, Journal of Photochemistry and Photobiology A: Chemistry 217 (2–3) (2011) 275–283.
[50] J.A. Galo, A. Soler-Illia, C. Sanchez, B. Lebeau, J. Patarin, Chemical Reviews 102 (2002) 4093–4138.
[51] Y. Liu, C. Liu, Z. Zhang, Chemical Engineering Journal 138 (2008) 596–601.
[52] G. Colón, M.C. Hidalgo, J.A. Navío, Applied Catalysis B: Environmental 45 (2003) 39–50.
[53] M.C. Hidalgo, M. Maicu, J.A. Navío, G. Colón, Catalysis Today 129 (2007) 43.
[54] E.A. Kozlova, T.P. Lyubina, M.A. Nasalevich, A.V. Vorontsov, A.V. Miller, V.V. Kaichev, V.N. Parmon, Catalysis Communications 12 (7) (2011) 597–601.
[55] M. Inagaki, R. Nonaka, B. Tryba, A.W. Morawski, Chemosphere 64 (2006) 437–445.
[56] G. Tian, H. Fu, L. Jing, C. Tian, Journal of Hazardous Materials 161 (2009) 1122–1130.
[57] N. Bálazs, K. Mogyorósi, D.F. Srankó, A. Pallagi, T. Alapi, A. Oszkó, A. Dombi, P. Sipos, Applied Catalysis B: Environmental 84 (2008) 356–362.
[58] Z. Ambrus, K. Mogyorosi, A. Szalai, T. Alapi, K. Demeter, A. Dombi, P. Sipos, Applied Catalysis A: General 340 (2) (2008) 153–161.
[59] J. Araña, J.M. Doña-Rodriguez, D. Portillo-Carrizo, C. Fernandez-Rodriguez, J. Perez-Peña, O. Gonzalez Diaz, J.A. Navio, M. Macias, Applied Catalysis B: Environmental 100 (2010) 346–354.
[60] M.C. Hidalgo, M. Maicu, J.A. Navío, G. Colon, Catalysis Today 129 (2007) 43–49.
[61] B. Sun, A.V. Vorontsov, P.G. Smirniotis, Langmuir 19 (2003) 3151–3156.
[62] C.A. Emilio, M.I. Litter, M. Kunst, M. Bouchard, C. Colbeau-Justin, Langmuir 22 (2006) 3606–3613.
[63] M. Dukkancı, G. Gunduz, Catalysis Communications 10 (2009) 913–919.
[64] C. Bernardini, G. Cappelletti, M.V. Dozzi, E. Selli, Journal of Photochemistry and Photobiology A: Chemistry 211 (2010) 185–192.